Mixed-Integer Predictive Control for a Three-Phase Electric Arc Furnace Producing Silico Manganese

Minh Tuan Dinh, Ionela Prodan, Olivier Lesage, Eduardo Mendes

2024 European Control Conference (ECC)
June 25-28, 2024. Stockholm, Sweden

Mixed-integer predictive control for a three-phase electric arc furnace producing Silico Manganese

Minh Tuan Dinh[1,2], Ionela Prodan[1], Olivier Lesage[2] and Eduardo Mendes[1]

***Abstract*— In the metallurgical industry, Electrical Arc Furnace (EAF) are usually controlled through simple rules, without necessarily handling the coupling among their various components leading to inefficiency in the operation (e.g., instability in multi-phase control, unbalanced power distribution). Herein, we first develop a mathematical model of the EAF which is able to capture the behavior of the three-phase electrical evolution in time. Then, we formulate a mixed-integer optimal control problem in an MPC (Model Predictive Control) framework for the plant's linearized model. The goals are to concurrently control power and intensity across the three phases to track a priori given set points, handle integer inputs and limit transformer tap switching frequency. This contributes to enhancing the furnace stability and energy efficiency. The approach is showcased over a three-phase furnace simulator developed by Eramet Ideas.**

***Index Terms*— Electric Arc Furnace (EAF), Electrical system, Transformer tap switching, Model Predictive Control (MPC), Mixed-Integer Programming (MIP).**

I. Introduction

Electric Arc Furnace (EAF) has been predominant for years in the metallurgical industry for the production of high-quality steel as well as essential alloys such as Ferro Manganese (FeMn), Ferro Silicon (FeSi), Silico Manganese (SiMn), etc. The 2023 report from Eurofer (European Steel Association) shows that 43.3% of EU crude steel production is now based on the EAF technology [1]. As a consequence, the innovation efforts on the EAF typically draw significant attention in the field. In particular, the integration of more advanced control systems, which can increase the furnace operation efficiency by optimizing the furnace production and satisfying the operating condition, is of great importance.

In an electric arc furnace or particularly a submerged arc furnace (e.g., SiMn furnace), where electrodes are deeply immersed in molten bath, most of the energy dissipated in the furnace comes from Joule heating effect [2]. Consequently, the control of furnace operation are considerably dependent on certain electrical information in the furnace (e.g., power consumption, electrode intensity, process resistance, etc). In the conventional control strategy, a three-phase EAF is commonly operated under monovariable power control to regulate the total active power of the three phases, whereas three-decoupling intensity controllers are utilized to manage the heat distribution inside the furnace bath. However, the approach shows some untreated limitations that are detrimental to the furnace operation. In particular, considering total power instead of multi-phase power may cause unbalanced power distribution across the three phases (i.e., dead-phase and live-phase phenomenon [3]), leading to uneven charge consumption, unequal refractory erosion and potential casting challenges due to frozen metal. Moreover, with three separated intensity controllers, the interaction effect (i.e., vertical displacement in one electrode affects the intensity in the other electrodes [3]) is incompletely taken into account which causes instability in the multi-phase control of intensity. These problems intensify with the low furnace power factor. Furthermore, no operating constraints are explicitly considered (e.g., maximum electrode intensity, maximum consumed power, tap changer switching frequency, etc [4]), hence, the furnace may power off due to the triggered safety.

In the research of EAF control systems, numerous studies have been conducted regarding the model formulation. In particular, the electrical system modeling of an EAF was initially raised in 1980 using an equivalent electrical circuit [3], [5]. The method was then developed in [6], [7] using Kirchhoff's laws to define a lumped impedance model describing essential elements in the electric circuit. However, the obtained results show a simple model of electrode intensities in which the three-phase powers from furnace transformers are not considered. Besides, various control techniques have been studied ranging from classical PI controllers [6], [8] to more advanced methods using adaptive control [7] or fuzzy control [9] to suppress intensity or resistance deviation in the electrodes based on the electrode positioning system. Model Predictive Control (MPC) is also employed in metallurgical control, highlighting its advantages of dealing with multi-input multi-output (MIMO) systems and handling multiple constraints [10], [11]. Recently, there has been increasing interest in the economic performance of the furnace using MPC method, in the sense of efficiently curtailing the energy cost and maximizing the profits [12], [13].

In spite of the huge benefits provided by the existing approaches, the electrical problems pertaining to the control of the EAF have not been comprehensively nor effectively tackled. Motivated by these shortcomings, in this paper, we:

i) describe a full electrical model of an EAF system through its electrical equivalent circuit (illustrated in Fig 1). This encompasses the dynamics of transformer tap position in three phases which has not been previously addressed, primarily due to the mandatory use of integer inputs. The coupling between phases due to electrode displacement is also captured in the dynamical model.

*This research has been financially supported by Eramet Ideas, Bpifrance and ANRT with a CIFRE fellowship granted to convention 2022/0866.

[1]Univ. Grenoble Alpes, Grenoble INP†, LCIS, F-26000, Valence, France, {minh-tuan.dinh,ionela.prodan,eduardo.mendes}@lcis.grenoble-inp.fr.

†Institute of Engineering and Management University Grenoble Alpes.

[2]Eramet Ideas, Trappes, France, olivier.lesage@eramet.com

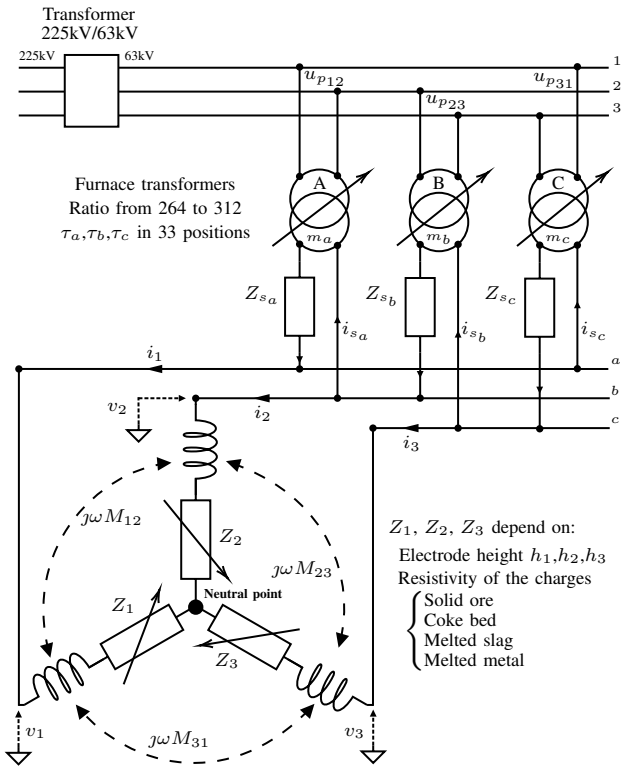

Fig. 1. Electrical equivalent circuit of a three-phase EAF system.

ii) consider a multi-phase control of both power and intensity while taking into account constraints related to integer inputs, tap switching frequency and output limits. These are integrated into an MPC optimization problem with real and integer variables and further validated using real-time data in a SiMn furnace simulator.

The rest of the paper is organized as follows. The model development in view of power and intensity control is described in section II. The constrained optimization problem is outlined in section III, while the assessment of the proposed control scheme is evaluated using real data and a simulator developed by Eramet Ideas in section IV. The conclusions and future works are discussed in section V.

Notation: Matrices and vectors are in bold uppercase and lowercase, respectively. $\mathbf{I_n}$ represents identity matrix of size n while $\mathbf{I_{n\times 1}}$ denotes column vector of ones. $\mathbf{0_{n\times m}}$ is the zeros matrix of size $n \times m$. $\odot$ denotes the element-wise multiplication. Furthermore, $\|\boldsymbol{x}\|^2_{\mathbf{Q}}$ denotes the weight norm $\boldsymbol{x}^\top \mathbf{Q}\boldsymbol{x}$, in which $\mathbf{x} \in \mathbb{R}^n$ is a vector and $\mathbf{Q} \in \mathbb{R}^{n\times n}$ is a positive semidefinite matrix. $|x|$ indicates the absolute value of x. $\mathbf{x}_{s|k}$ and $\mathbf{u}_{s|k}$ represent the state and input at time step k, given the information available upon the predicted step s.

II. EAF MODEL IN VIEW OF CONTROL

Fig. 1 illustrates the electrical equivalent diagram of an electric arc furnace with 63 kV input voltage taken from the 225 kV electrical grid through a step-down transformer. In the circuit, the modeling of the EAF electrical system is divided into two main parts, i.e., transformer-to-cables modeling and electrode-to-bath modeling. The electrical elements presented in the circuit are described in detail in Table I.

TABLE I
DESCRIPTION OF ELECTRICAL ELEMENTS IN THE EQUIVALENT CIRCUIT

Symbol$^{(*)}$	**Description**	**Unit**
$u_{p_{12}}$, $u_{p_{23}}$, $u_{p_{31}}$ v_1, v_2, v_3	primary transformer voltage electrode-to-bath voltage	[V]
i_{s_a}, i_{s_b}, i_{s_c} i_1, i_2, i_3	secondary transformer intensity electrode-to-bath intensity	[A]
Z_{s_a}, Z_{s_b}, Z_{s_c} Z_1, Z_2, Z_3 $j\omega[M_{12}, M_{23}, M_{31}]$	transformer-to-cable impedance electrode-to-bath impedance electrode mutual inductance $^{(**)}$	[Ω]
m_a, m_b, m_c	transformer ratio	-
τ_a, τ_b, τ_c	transformer tap changer position	-
h_1, h_2, h_3	electrode position	[m]

$^{(*)}$ subscripts $_{1,2,3}$ or $_{a,b,c}$ denote the phase order in the electrical system.
$^{(**)}$ $\omega = 2\pi f$ with $f = 50$Hz is the power line frequency.

A. The transient model

Since the modeling of the electrical system is obtained from the equivalent circuit in Fig. 1, the transient model of the furnace can be derived by electrical analysis using Ohm's law and Kirchoff's law applied to the circuit. In the first phase, we have a relation between the primary and secondary sides of the transformer A as follows:

$$u_{p_{12}} = m_a(u_{ab} + Z_{s_a} i_{s_a}), \tag{1}$$

where u_{ab} denotes the voltage between line a and b on the secondary side and i_{s_a} represents the secondary intensity. We apply the Ohm's law to formulate the electrode-to-bath voltages (electrode head voltages) in line a and b:

$$\begin{aligned} v_1 &= Z_1 i_1 + j\omega M_{12} i_2 + j\omega M_{31} i_3, \\ v_2 &= Z_2 i_2 + j\omega M_{23} i_3 + j\omega M_{12} i_1. \end{aligned} \tag{2}$$

From this, the voltages between line a and b can be found by the subtraction of individual head voltages v_1 and v_2:

$$u_{ab} = v_1 - v_2. \tag{3}$$

By incorporating (1) and (2) into (3), we gain an expression of the secondary intensity i_{s_a} in the first phase:

$$\begin{aligned} Z_{s_a} i_{s_a} = \frac{u_{p_{12}}}{m_a} &+ (Z_1 - j\omega M_{12}) i_1 \\ &- (Z_2 - j\omega M_{12}) i_2 + (j\omega M_{31} - j\omega M_{23}) i_3. \end{aligned} \tag{4}$$

Similarly, the secondary intensity i_{s_c} of the third phase is:

$$\begin{aligned} Z_{s_c} i_{s_c} = \frac{u_{p_{31}}}{m_c} &+ (Z_1 - j\omega M_{31}) i_1 \\ &- (j\omega M_{23} - j\omega M_{12}) i_2 + (Z_3 - j\omega M_{31}) i_3. \end{aligned} \tag{5}$$

Next, we apply the Kirchhoff's current law at the node of line a taking into account a pair of secondary intensities (i_{s_a}, i_{s_c}) in phase 1 and phase 3 to retrieve the relation:

$$i_1 = i_{s_a} - i_{s_c}. \tag{6}$$

Employing (4) and (5) into (6) removes the presence of secondary intensities in the following formulation:

$$\begin{aligned}&\Big[Z_{s_a}Z_{s_c} + Z_{s_c}(Z_1 - \jmath\omega M_{12}) - Z_{s_a}(Z_1 - \jmath\omega M_{31})\Big] i_1 \\ &-\Big[Z_{s_c}(Z_2 - \jmath\omega M_{12}) + Z_{s_a}(\jmath\omega M_{23} - \jmath\omega M_{12})\Big] i_2 \\ &+\Big[Z_{s_c}(\jmath\omega M_{31} - \jmath\omega M_{23}) - Z_{s_a}(Z_3 - \jmath\omega M_{31})\Big] i_3 \\ &= u_{p_{12}}\frac{Z_{s_c}}{m_a} - u_{p_{31}}\frac{Z_{s_a}}{m_c}.\end{aligned} \tag{7}$$

Here, we obtain the expression of electrode-to-bath intensities (i_1, i_2, i_3) flowing from each of the three electrodes through the furnace charges to the neutral floating point at the bottom of furnace. Similarly, we apply the electrical analysis using Kirchhoff's current law to line b taking into account a pair of intensities (i_{s_b}, i_{s_a}) in phase 2 and 1 to derive:

$$\begin{aligned}&\Big[Z_{s_a}(\jmath\omega M_{12} - \jmath\omega M_{31}) - Z_{s_b}(Z_1 - \jmath\omega M_{12})\Big] i_1 \\ &+\Big[Z_{s_b}Z_{s_a} + Z_{s_a}(Z_2 - \jmath\omega M_{23}) - Z_{s_b}(Z_2 - \jmath\omega M_{12})\Big] i_2 \\ &-\Big[Z_{s_a}(Z_3 - \jmath\omega M_{23}) + Z_{s_b}(\jmath\omega M_{31} - \jmath\omega M_{23})\Big] i_3 \\ &= u_{p_{23}}\frac{Z_{s_a}}{m_b} - u_{p_{12}}\frac{Z_{s_b}}{m_a}.\end{aligned} \tag{8}$$

Lastly, the Kirchhoff's current law takes effect into the electrical neutral point which corresponds to the virtual floating point in the bottom hearth of the furnace. This yields the connection among the three electrode-to-bath intensities:

$$i_1 + i_2 + i_3 = 0. \tag{9}$$

Together, the equations (7), (8) and (9) describe the EAF electrical system. This can be expressed as follows:

$$\mathbf{F}\mathbf{i} = \mathbf{q}, \tag{10}$$

where the vector $\mathbf{i} \triangleq [i_1\ i_2\ i_3]^\top \in \mathbb{C}^3$ denotes the electrode-to-bath intensities; the matrices $\mathbf{F} \in \mathbb{C}^{3\times3}$ and $\mathbf{q} \in \mathbb{C}^3$ are given by the coefficients on the left and right-hand sides, respectively, from the set of equations (7), (8) and (9).

Moreover, the transformer ratio $\mathbf{m} \triangleq [m_a\ m_b\ m_c]^\top \in \mathbb{R}^3$ and the impedance $\mathbf{z_s} \triangleq [Z_{s_a}\ Z_{s_b}\ Z_{s_c}]^\top \in \mathbb{C}^3$ are regulated by a specific device within the transformer known as tap changer. The position of the tap changer $\boldsymbol{\tau} \triangleq [\tau_a\ \tau_b\ \tau_c]^\top \in {\mathbb{Z}_+}^3$ ranges in discrete steps due to its physical design. The regulation is described by the univariate mapping functions:

$$m_j = f_1(\tau_j), \tag{11}$$

$$Z_{s_j} = f_2(\tau_j), \tag{12}$$

where j taken from {a,b,c} denotes the phase order and $f_1(\cdot), f_2(\cdot) : \mathbb{Z}_+ \mapsto \mathbb{R}, \mathbb{C}$ are quadratic polynomials defined using the manufacturer's specifications or experimental tests.

Furthermore, the active power contributed to the process, which includes the electrode powers and the furnace bath powers can be derived as follows:

$$\mathbf{p} = \mathbf{r} \odot |\mathbf{i}|^2, \tag{13}$$

where, $\mathbf{p} \triangleq [P_1\ P_2\ P_3]^\top \in \mathbb{R}^3$ denotes the electrode-to-bath active powers, $\mathbf{r} \triangleq \Re(\mathbf{z}) = [R_1\ R_2\ R_3]^\top \in \mathbb{R}^3$ represents the electrode-to-bath resistances. From equations (10)-(13), it is apparent that both power and intensity depend on certain key elements, which will be treated as the states of the system, namely, tap changer position $\boldsymbol{\tau}$ and electrode-to-bath impedance denoted as $\mathbf{z} \triangleq [Z_1\ Z_2\ Z_3]^\top \in \mathbb{C}^3$.

B. The EAF dynamics

Drawing insights from the above subsection, we consider tap variation as a decision variable, thus, the evolution of the tap changer position at a time step k is defined as follows:

$$\boldsymbol{\tau}_{k+1} = \boldsymbol{\tau}_k + \boldsymbol{\delta\tau}_k, \tag{14}$$

where $\boldsymbol{\delta\tau} \triangleq [\delta\tau_a\ \delta\tau_b\ \delta\tau_c]^\top \in \mathbb{Z}^3$ refers to the tap changer variation which is inherently discrete due to the integer-based nature of tap changer position $\boldsymbol{\tau}$. Moreover, the dynamics of electrode-to-bath impedance is mainly influenced by the vertical displacements of the three electrode positions. Hence, an approximation model depicting how the electrode displacements impact the electrode-to-bath impedance has been developed using measurement analysis on the plant:

$$\underbrace{\begin{bmatrix}\delta Z_1\\ \delta Z_2\\ \delta Z_3\end{bmatrix}}_{\boldsymbol{\delta z}_k} = \underbrace{\begin{bmatrix}\gamma_1 & 0 & 0\\ 0 & \gamma_2 & 0\\ 0 & 0 & \gamma_3\end{bmatrix}}_{\boldsymbol{\Gamma}_{3\times3}} \underbrace{\begin{bmatrix}\delta h_1\\ \delta h_2\\ \delta h_3\end{bmatrix}}_{\boldsymbol{\delta h}_k}, \tag{15}$$

where $\boldsymbol{\delta z} \in \mathbb{C}^3$ represents the electrode-to-bath impedance variation with respect to the electrodes height deviations $\boldsymbol{\delta h} \in \mathbb{R}^3$. The relation between $\boldsymbol{\delta z}$ and $\boldsymbol{\delta h}$ is described by the diagonal matrix $\boldsymbol{\Gamma} \in \mathbb{C}^{3\times3}$ in which its diagonal elements γ_1, γ_2, γ_3 are estimated from measurement data during the furnace operation. The dynamics shows an assumption that vertical electrode displacement within one phase is directly proportional to the electrode-to-bath impedance within that same phase while resulting in no influence on other phases impedances (e.g., $\delta Z_1 \notin \{\delta h_2, \delta h_3\}$). Besides, the electrode position $\mathbf{h} \triangleq [h_1\ h_2\ h_3]^\top$ at time step k is determined by:

$$\mathbf{h}_{k+1} = \mathbf{h}_k + \boldsymbol{\delta h}_k. \tag{16}$$

It is also worth noting that the electrode-to-bath impedances in the three phases are considerably influenced by the states of burden inside the furnace bath as mentioned in Fig. 1.

Finally, to obtain the discrete model of the EAF electrical system used for control design, we combine the equations (10)-(13) and take into account the dynamics (14) and (15):

$$\mathbf{x}_{k+1} = \mathbf{A^d}\,\mathbf{x}_k + \mathbf{B^d}\,\mathbf{u}_k, \tag{17a}$$

$$\mathbf{y}_k = g(\mathbf{x}_k), \tag{17b}$$

where $\mathbf{x}_k \triangleq [\mathbf{z}\ \boldsymbol{\tau}]^\top \in \mathbb{C}^3 \times \mathbb{Z}_+^3$, $\mathbf{y}_k \triangleq [\mathbf{p}\ |\mathbf{i}|]^\top \in \mathbb{R}^6$, represent the electrical system states and outputs, $\mathbf{u}_k \triangleq [\boldsymbol{\delta\tau}\ \ \boldsymbol{\delta h}]^\top \in \mathbb{Z}^3 \times \mathbb{R}^3$ is the control input, $\mathbf{A^d} \triangleq \mathbf{I_6}$ and $\mathbf{B^d} \triangleq \begin{bmatrix}\mathbf{0_{3\times3}} & \boldsymbol{\Gamma}_{3\times3}\\ \mathbf{I_3} & \mathbf{0_{3\times3}}\end{bmatrix} \in \mathbb{C}^{6\times6}$. The function $g(\cdot)$: $\mathbb{C}^3 \times \mathbb{Z}_+^3 \mapsto \mathbb{R}^6$ is strongly nonlinear and retrieved from

equations (10)-(13). It indicates that the system outputs (i.e., power and intensity) depend nonlinearly on the system states (i.e., impedance and transformer tap position).

In the sequel, for linear control design, we consider the linearization problem of the nonlinear discrete model in (17). Applying Taylor's expansion in a neighborhood of the operating state $\mathbf{x}_k$ at k-th time step, we have the following Taylor decomposition:

$$\begin{aligned} g(\mathbf{x}_{k+1}) &= g(\mathbf{x}_k) + \frac{\partial g}{\partial \mathbf{x}}\Big|_{\mathbf{x}_k} (\mathbf{x}_{k+1} - \mathbf{x}_k) + R_n \\ &= g(\mathbf{x}_k) + \mathbf{B^f}\,\mathbf{u}_k + R_n, \end{aligned} \tag{18}$$

where the matrix $\mathbf{B^f} \in \mathbb{R}^{6\times 6}$ stands for the interaction factors in the system. In other words, it represents how the tap changer movement and electrode deviation in each phase will affect the powers and intensities in all three phases:

$$\mathbf{B^f} \triangleq \frac{\partial g}{\partial \mathbf{x}}\Big|_{\mathbf{x}_k} \mathbf{B^d}. \tag{19}$$

This helps the prediction model to take into consideration the interaction effect among the phases. Besides, $R_n \in \mathbb{R}^6$ represents the higher other terms in the Taylor expansion with terms of order $n > 1$. By ignoring R_n (a reasonable assumption near the linearization point), (18) gives us the linearized model of electrode-to-bath power and intensity. Moreover, to keep track of the electrode position for handling the actuator constraints, we also take into account the model of electrode position (16). So, the dynamics (17) can be rewritten as a discrete linear time-variant model as follows:

$$\boldsymbol{x}_{k+1} = \boldsymbol{A}\boldsymbol{x}_k + \boldsymbol{B}_k\boldsymbol{u}_k, \tag{20a}$$

$$\boldsymbol{y}_k = \boldsymbol{C}\boldsymbol{x}_k, \tag{20b}$$

where , $\boldsymbol{x}_k \triangleq [\mathbf{p}\ |\mathbf{i}|\ \mathbf{z}\ \boldsymbol{\tau}\ \mathbf{h}]^\top \in \mathbb{C}^{15}$ denotes the augmented state vector, whereas the output $\boldsymbol{y}_k \in \mathbb{R}^6$ and the input $\boldsymbol{u}_k \in \mathbb{R}^6$ remain the same compared to (17). Furthermore, $\boldsymbol{A} \triangleq \mathbf{I_{15}}$ is the identity matrix, $\boldsymbol{B}_k \triangleq [\mathbf{B^f}\ \mathbf{B^d}\ [\mathbf{0_{3\times 3}}\ \mathbf{I_3}]]^\top \in \mathbb{C}^{15\times 6}$ is a time-varying matrix and $\boldsymbol{C} \triangleq [\mathbf{I_6}\ \mathbf{0_{6\times 9}}] \in \mathbb{R}^{6\times 15}$.

III. Mixed-Integer Model Predictive Control

The main goal is to enhance the productivity of the EAF operation. To achieve this, the control design must focus on two crucial factors: the power contribution in three phases and the heat distribution in the furnace bath. Accordingly, we construct a multi-phase control design involving 6 variables: three electrode-to-bath powers and three electrode-to-bath intensities across the three phases. The objective is to reduce the error between their measured values and their references $\boldsymbol{y}^{\mathbf{r}} \triangleq [\mathbf{p^r},\ |\mathbf{i^r}|] \in \mathbb{R}^6$. This approach ensures that with well-predefined profiles of power and intensity, the reference tracking of these variables can lead to a productive operation. Moreover, to ensure the safety and smooth operation of the system, furnace operating conditions are also taken into account in the control approach, specifically, electrode current limit[1] ($|\mathbf{i_{ub}}|$), maximum consumed power ($\mathbf{p_{ub}}$), resistance boundary ($\mathbf{r_{lb}}, \mathbf{r_{up}}$), reactance boundary ($\mathbf{x_{lb}}, \mathbf{x_{up}}$), tap changer range ($\boldsymbol{\tau}_{\mathbf{lb}}, \boldsymbol{\tau}_{\mathbf{ub}}$), electrode position range ($\mathbf{h_{lb}}, \mathbf{h_{up}}$), all gathered in the state constraint set:

$$\begin{aligned} \mathcal{X} \triangleq \{&0 \le \mathbf{p} \le \mathbf{p_{ub}},\ 0 \le |\mathbf{i}| \le |\mathbf{i_{ub}}|, \\ &\mathbf{r_{lb}} \le \Re(\mathbf{z}) \le \mathbf{r_{ub}},\ \mathbf{x_{lb}} \le \Im(\mathbf{z}) \le \mathbf{x_{ub}}, \\ &\boldsymbol{\tau}_{\mathbf{lb}} \le \boldsymbol{\tau} \le \boldsymbol{\tau}_{\mathbf{ub}},\ \mathbf{h_{lb}} \le \mathbf{h} \le \mathbf{h_{ub}}\}. \end{aligned} \tag{21}$$

Furthermore, considering the physical limitations of the actuators and the local approximation assumption of the linearized model in (20), restrictions are imposed on the control inputs. Particularly, constraints are defined for the tap changer variation, ($\boldsymbol{\Delta\tau_b}$), and the electrode height variation, ($\mathbf{\Delta h_b}$), within the input constraint set:

$$\mathcal{U} \triangleq \{|\boldsymbol{\delta\tau}| \le \boldsymbol{\Delta\tau_b},\ |\delta\mathbf{h}| \le \mathbf{\Delta h_b}\}. \tag{22}$$

Additionally, concerning the tap changer switching mechanism, frequent adjustments in the tap position are strongly discouraged to avoid undesirable consequences in terms of cost and technical performance of the transformers. Because higher demands of the tap changer switching in a short period gradually lead to the earlier maintenance of the transformer or even mechanical failure of the tap changer devices. As a result, this operating condition is also considered in our approach and will be addressed in the optimization problem.

Next, we propose a mixed-integer MPC formulation [14], solved over the prediction horizon N_p at every time step k:

$$\arg \min_{\boldsymbol{v},\boldsymbol{u}\left(\substack{\boldsymbol{\delta\tau}\\ \boldsymbol{\delta h}}\right)} \sum_{s=0}^{N_p-1} \ell_1(\boldsymbol{y}_{s|k}, \boldsymbol{y}^{\mathbf{r}}_{s|k}) + \ell_2(\boldsymbol{v}_{s|k}) \tag{23a}$$

$$\begin{aligned} \text{s.t.}\quad & \forall s \in [0,\ N_p - 1]: \\ & \boldsymbol{x}_{s+1|k} = \boldsymbol{A}\boldsymbol{x}_{s|k} + \boldsymbol{B}_k\boldsymbol{u}_{s|k}, && \text{(23b)} \\ & \boldsymbol{y}_{s+1|k} = \boldsymbol{C}\boldsymbol{x}_{s+1|k},\ \boldsymbol{x}_{0|k} = \boldsymbol{x}_{\mathbf{0}}, && \text{(23c)} \\ & \boldsymbol{x}_{s+1|k} \in \mathcal{X},\ \boldsymbol{u}_{s|k} \in \mathcal{U},\ \boldsymbol{\delta\tau}_{s|k} \in \mathbb{Z}^3, && \text{(23d)} \\ & |\boldsymbol{\delta\tau}_{s|k}| \le \mathrm{L}\boldsymbol{v}_{s|k},\ \boldsymbol{v}_{s|k} \in \{0,1\}^3. && \text{(23e)} \end{aligned}$$

The solution of (23) provides the optimal sequences of $\boldsymbol{v}^*_k = \{\boldsymbol{v}^*_{0|k}, \ldots, \boldsymbol{v}^*_{N_p-1|k}\}$ and $\boldsymbol{u}^*_k = \{\boldsymbol{u}^*_{0|k}, \ldots, \boldsymbol{u}^*_{N_p-1|k}\}$. At each sample time k, the control input is taken as $\boldsymbol{u}^*_{0|k}$. In (23), $\boldsymbol{v}_{s|k} \in \{0,1\}^3$ is defined as the auxiliary binary vector. The objective (23a) includes the sum of two quadratic cost functions $\ell_1(\cdot)$ and $\ell_2(\cdot)$ over the prediction step $s \in [0,\ N_p - 1]$. Here, the stage cost $\ell_1(\cdot)$ is defined as:

$$\ell_1 \triangleq \left\| \boldsymbol{y}_{s+1|k} - \boldsymbol{y}^{\mathbf{r}}_{s+1|k} \right\|^2_{\mathbf{Q}}, \tag{24}$$

to penalize the tracking errors of the electrode-to-bath power and intensity with respect to the desired references across all three phases. The cost is in quadratic form with the symmetric weighting matrices $\mathbf{Q} \in \mathbb{R}^{6\times 6}$ (positive semidefinite) defined by the users. The switching cost $\ell_2(\cdot)$ described by:

$$\ell_2 \triangleq \left\| \boldsymbol{v}_{s|k} \right\|^2_{\mathbf{V}\odot\boldsymbol{\lambda}_k}, \tag{25}$$

is used instead of penalizing the input cost to effectively reduce the switching frequency of the tap changer in the

[1]It is worth noting that the maximum electrode current is of great importance since excessive currents passing the electrodes results in an abnormally high incidence of electrode breakages [4].

transformers. The idea here is to employ the binary variable vector $\boldsymbol{v}$ in the cost $\ell_2(\cdot)$ in conjunction with the constraint (23e) to proactively manage the tap movement frequency. The cost is penalized through a time-varying weighting factor defined by the matrix $\mathbf{V} \in \mathbb{R}^{3\times3}$ and the vector $\boldsymbol{\lambda}_k \in \mathbb{R}^3$.

The weighting parameter $\boldsymbol{\lambda}_k$ in (25) is tuned online using Algorithm 1 to adjust the importance given to the switching cost $\ell_2(\cdot)$ at every time step k, thereby obtaining a reasonable value for $\boldsymbol{v}_{s|k}$. More specifically, the idea is to assign a maximum value $\boldsymbol{\lambda}_\mathbf{m}$ to $\boldsymbol{\lambda}_k$ as soon as the tap changer switching occurs, ensuring that the return value of $\boldsymbol{v}_{s|k}$ will be zero. Together with constraint (23e), this blocks the tap changer switching. Otherwise, the power errors between the output $\mathbf{p}_k$ and the reference $\mathbf{p^r}_k$ are consecutively accumulated and transformed into the cumulative energy errors $\mathbf{E}_{err|k}$ over the corresponding interval. Then, $\boldsymbol{\lambda}_k$ is decreased by these accumulated energy terms along with a tuning parameter μ, which determines the rate of the accumulation. Decreasing $\boldsymbol{\lambda}_k$ to a sufficiently small amount will facilitate tap switching at a certain level by allowing nonzero values for $\boldsymbol{v}_{s|k}$.

Furthermore, the constraints (23b) and (23c) describe the discrete linear model (20) in which the vector $\boldsymbol{x_0}$ denotes the initial state retrieved from the measurement system. The state constraint set $\mathcal{X}$ and input constraint set $\mathcal{U}$ shown in (23d) are detailed in (21) and (22). The constraint (23d) is an integer condition of the tap changer movement variable $\boldsymbol{\delta\tau}$. Finally, the constraint (23e) is used to disable or activate the tap switching ability in the range of $\mathrm{L} \leq \boldsymbol{\Delta\tau_b}$. More specifically, each element in $\boldsymbol{\delta\tau}_{s|k}$ is constrained to zero if the corresponding element in $\boldsymbol{v}_{s|k}$ is zero, no matter what the value of L is, otherwise, it allows the optimizer to choose any value for $\boldsymbol{\delta\tau}_{s|k}$ in range [-L L].

Algorithm 1: Online tuning of coefficient λ for the cost switching based on the accumulated energy error.

Input: optimal variable $\boldsymbol{v}^*_{0|k-1}$, rate μ, weight $\boldsymbol{\lambda}_\mathbf{m}$.
Output: weighting coefficient $\boldsymbol{\lambda}_k$ in (25).
if $\boldsymbol{v}^*_{0|k-1} = 0$ **then**
  $\mathbf{E}_{err|k} \leftarrow \mathbf{E}_{err|k-1} + (\mathbf{p}_k - \mathbf{p^r}_k)\Delta_t$; /* Δ_t is the sampling time */
  $\boldsymbol{\lambda}_k \leftarrow \max\{0, \boldsymbol{\lambda}_\mathbf{m} - \mu \cdot \mathbf{E}_{err|k}\}$; /* μ is cumulative rate */
else
  $\mathbf{E}_{err|k} \leftarrow 0$;
  $\boldsymbol{\lambda}_k \leftarrow \boldsymbol{\lambda}_\mathbf{m}$
end

IV. Simulations

In here, we validate the control approach outlined in Section III using a SiMn simulator developed by Eramet Ideas taking numerical data from the real plant. The simulation was implemented in Python 3.9 using CasADi modeling language and Bonmin mixed-integer programming solver [15], [16]. All the computations were executed on a Dell Optiplex 7060 desktop with an Intel Core i7-8700 3.20 GHz CPU.

TABLE II
Parameter for the optimization-based control of the EAF.

Symbol	Numerical value	Unit
Controller		
$\mathbf{Q}$	$\begin{bmatrix} 10^{-5}\mathbf{I_3} & \mathbf{0_{3\times3}} \\ \mathbf{0_{3\times3}} & 10^{4}\mathbf{I_3} \end{bmatrix}$	-
$\mathbf{V}$	$\mathbf{I_3}$	-
N_p	2	[steps]
$\boldsymbol{\lambda_m}$	$10^{11}\mathbf{I_{3\times1}}$	-
μ	10^4	-
Constraint		
$\mathbf{p_{ub}}$, $\lvert\mathbf{i_{ub}}\rvert$	$15\mathbf{I_{3\times1}}, 145\mathbf{I_{3\times1}}$	[MW], [kA]
$\mathbf{r_{lb}}$, $\mathbf{r_{ub}}$	$0.165\mathbf{I_{3\times1}}, 2\mathbf{I_{3\times1}}$	[mΩ], [mΩ]
$\mathbf{x_{lb}}$, $\mathbf{x_{ub}}$	$0.225\mathbf{I_{3\times1}}, 2\mathbf{I_{3\times1}}$	[mΩ], [mΩ]
$\boldsymbol{\tau_{lb}}$, $\boldsymbol{\tau_{ub}}$	$\mathbf{I_{3\times1}}, 33\mathbf{I_{3\times1}}$	[$steps$], [$steps$]
$\mathbf{h_{lb}}$, $\mathbf{h_{ub}}$	$5\mathbf{I_{3\times1}}, 105\mathbf{I_{3\times1}}$	[cm], [cm]
$\boldsymbol{\Delta\tau_b}$, $\boldsymbol{\Delta h_b}$	$5\mathbf{I_{3\times1}}, 5\mathbf{I_{3\times1}}$	[$steps$], [cm]
Objective		
$\mathbf{p^r}$, $\lvert\mathbf{i^r}\rvert$	$10\mathbf{I_{3\times1}}, 127\mathbf{I_{3\times1}}$	[MW], [kA]
ϵ_p, ϵ_i	0.5, 0.5	[MW], [kA]

Hereinafter, we present the simulation results of electrode-to-bath power and intensity tracking across all three phases, achieved through solving the optimization problem (23) with predefined references $\{\mathbf{p^r}, \lvert\mathbf{i^r}\rvert\}$ and acceptable tracking errors or tracking tolerances determined by $\{\epsilon_p, \epsilon_i\}$:

$$\begin{aligned} \mathcal{T}_p &\triangleq \mathbf{p^r} \pm \epsilon_p, \\ \mathcal{T}_i &\triangleq \lvert\mathbf{i^r}\rvert \pm \epsilon_i. \end{aligned} \tag{26}$$

The numerical control parameters used for the simulation are shown in Table II with control sampling time Δ_t = 4 (s). The mean computation time of the controller at each sample time is 1.07 (s) which is reasonable for the choice of Δ_t.

The simulation results were given after 1.5 hours of simulation and illustrated in Fig 2 where the input, output and impedance are plotted in order. In particular, Fig 2(a) demonstrates that the output performances in the three phases (in red, blue and green lines, respectively) all converge to the targets (in pink dotted line) and almost remain within tracking tolerance ranges $\mathcal{T}_p$, $\mathcal{T}_i$ (in orange dashed lines). Notably, the electrical environment is also affected by various factors during the operation. For instance, some significant variations in the power and sudden intensity drops occur due to the casting events of the furnace (magnified in the figure), during which the liquid metal and slag are poured out, hence the conductivity in the bath is considerably decreased. Besides, some overshoots in intensity level are detected which can be explained by the increase of the tap changer position to compensate for the power drop. We underline that the MPC algorithm always respects the maximum power and intensity constraints $\{\mathbf{p_{ub}}, \lvert\mathbf{i_{ub}}\rvert\}$ as given in Table II.

Moreover, as shown in Fig 2(b), the commands on the electrode displacement (orange circle) are significantly required compared to the switching in the tap changer device (blue square). Here, we can also observe that the values of tap changer variation are given in discrete steps, with the mean number of switching in three phases counted 19 times.

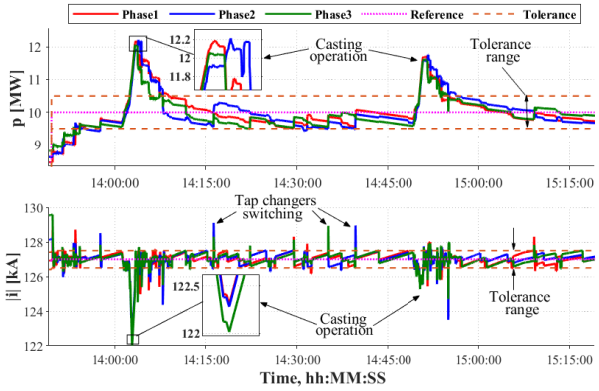

(a) Tracking performance of power (upper) and intensity (lower).

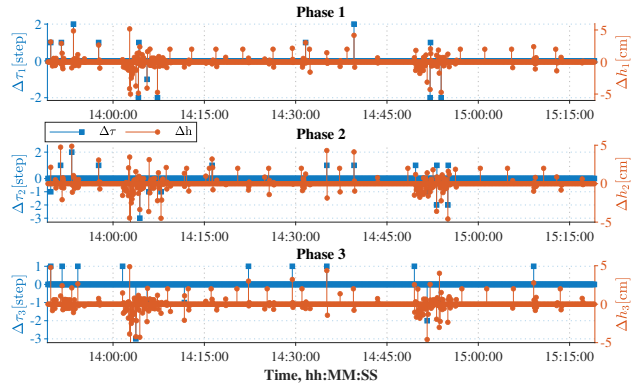

(b) Tap changer movement and electrode height variation.

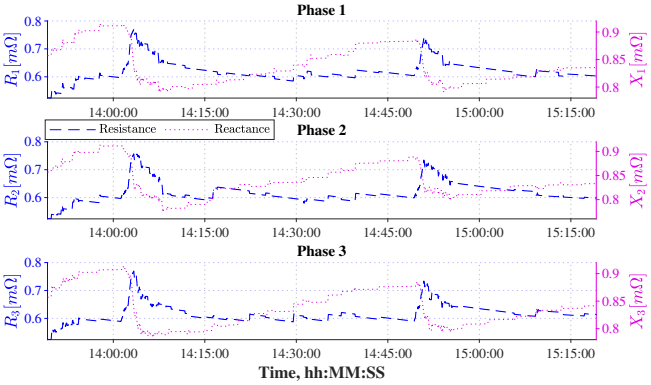

(c) Total resistance and reactance in the electrodes and molten bath.

Fig. 2. MIQP-based MPC test on furnace simulator (during 1.5 hours) for electrode-to-bath power and intensity control in three phases (scenario 1).

Lastly, Fig 2(c) illustrates the evolution of electrode-to-bath impedance during the furnace operation. Notably, attention should be paid to the impedance behaviors occurring separately from the casting events. Particularly, the resistance (shown in navy dash lines) remains nearly consistent around $0.6 - 0.61$ ($m\Omega$), while the reactance (indicated by magenta dot lines) increases proportionally with time.

To showcase the significance of including the cost (25) and constraint (23e) in reducing the frequency of tap changer switching, we conducted another scenario in which we solved the optimization problem (23) without these elements. This resulted in a higher number of tap switches, averaging 32.2 times in 1.5 hours of simulation, compared to 19 times in the initial scenario. As expected, the computation time of the optimization problem in the second scenario is less than in the first scenario (0.68s versus 1.07s) due to the decrease in the complexity of the problem.

V. Conclusion

In this work, we provided an approach that takes advantage of Model Predictive Control (MPC) combined with mixed-integer programming (MIP) to establish the electrical control system for an Electric Arc Furnace (EAF). Modeling of the electrical elements in the EAF system was obtained by analyzing the equivalent circuit. Afterwards, a validated furnace simulator was used to evaluate the performance of the multi-phase power and intensity controller. The future goal is to experimentally test the algorithm on the real plant.

References

[1] Eurofer, *Statistical handbook: European steel in figures 2023*. Brussels: European Steel Association, 2023.

[2] J. Jones, B. Bowman, and P. Lefrank, "Electric furnace steelmaking," in *The Making, Shaping and Treating of Steel*, R. Fruehan, Ed. Pittsburgh: The AISE Steel Foundation, 1998, pp. 525–660.

[3] I. Barker and A. Stewart, "Inductive reactance and the operation of large submerged-arc furnaces," *Journal of the Southern African Institute of Mining and Metallurgy (JSAIMM)*, vol. 80, no. 3, pp. 123–128, 1980.

[4] A. De Waal, U. Barker, M. Rennie, J. Klopper, and B. Groeneveld, "Electrical factors affecting the economic optimization of submerged-arc furnaces," in *INFACON 6. Proceedings of the 6th International Ferroalloys Congress*, Cape Town, South Africa, 1992, pp. 247–252.

[5] I. Barker, "An electrode controller for submerged arc furnaces," *IFAC Proceedings Volumes*, vol. 13, no. 7, pp. 611–621, 1980, proceedings of the 3rd IFAC Symposium on Automation in Mining, Mineral, and Metal Processing.

[6] B. Boulet, G. Lalli, and M. Ajersch, "Modeling and control of an electric arc furnace," in *Proceedings of the 2003 American Control Conference.*, vol. 4, 2003, pp. 3060–3064.

[7] R. Balan, O. Hancu, and E. Lupu, "Modeling and adaptive control of an electric arc furnace," *IFAC Proceedings Volumes*, vol. 40, no. 8, pp. 163–168, 2007.

[8] A. S. Hauksdóttir, A. Gestsson, and A. Vésteinsson, "Current control of a three-phase submerged arc ferrosilicon furnace," *Control Engineering Practice*, vol. 10, no. 4, pp. 457–463, 2002.

[9] M. Moghadasian and E. Alenasser, "Modelling and artificial intelligence-based control of electrode system for an electric arc furnace," *Journal of Electromagnetic Analysis and Applications*, 2011.

[10] J. Bekker, I. Craig, and P. Pistorius, "Model predictive control of an eaf off-gas process," *IFAC Proceedings Volumes*, vol. 32, no. 2, pp. 7050–7055, 1999.

[11] L. Coetzee, I. Craig, and L. Rathaba, "Mpc control of the refining stage of an electric arc furnace," *IFAC proceedings volumes*, vol. 38, no. 1, pp. 151–156, 2005.

[12] M. M. Rashid, P. Mhaskary, and C. L. Swartz, "Economic model predictive control of the electric arc furnace using data-driven multi-rate models," in *American Control Conference (ACC)*, 2016.

[13] S. Shyamal and C. L. Swartz, "Real-time energy management for electric arc furnace operation," *Journal of Process Control*, vol. 74, pp. 50–62, 2019.

[14] I. Prodan, F. Stoican, S. Olaru, and S.-I. Niculescu, *Mixed-Integer Representations in Control Design*. Springer, 2016.

[15] J. A. Andersson, J. Gillis, G. Horn, J. B. Rawlings, and M. Diehl, "Casadi: a software framework for nonlinear optimization and optimal control," *Mathematical Programming Computation*, vol. 11, 2019.

[16] P. Bonami, L. T. Biegler, A. R. Conn, G. Cornuéjols, I. E. Grossmann, C. D. Laird, J. Lee, A. Lodi, F. Margot, N. Sawaya *et al.*, "An algorithmic framework for convex mixed integer nonlinear programs," *Discrete optimization*, vol. 5, no. 2, pp. 186–204, 2008.